

Research Article

Model-Based Leakage Estimation and Remaining Useful Life Prediction of Control Gas Cylinder

Zhenzhen Zhang ¹, Hui Chen ^{1,2}, Chao Qi ¹ and Yazhou Liu ¹

¹*Xi'an Aerospace Propulsion Institute, Xi'an 710000, China*

²*School of Mechanical Engineering, Xi'an Jiaotong University, Xi'an 710000, China*

Correspondence should be addressed to Hui Chen; chenhui2013abc@163.com

Received 22 December 2022; Revised 7 April 2023; Accepted 10 April 2023; Published 9 May 2023

Academic Editor: Qingfei Fu

Copyright © 2023 Zhenzhen Zhang et al. This is an open access article distributed under the Creative Commons Attribution License, which permits unrestricted use, distribution, and reproduction in any medium, provided the original work is properly cited.

The high-pressure gas cylinder is the pressure source for liquid propellant engine valve control. Leakage is a significant cause of pressure loss in gas cylinders, leading to engine control failure and serious flight accidents. In this paper, a model-based approach to estimate the leakage area and remaining useful life (RUL) of gas cylinders is proposed. To estimate the leakage area, a state space representation of the cylinder system is developed based on the nonlinear model derived from momentum, energy, and continuity equations. Leakage is defined as a system state, and an extended Kalman filter (EKF) as a state observer is implemented to estimate the leakage area. Internal pressure measurements of the gas cylinder are required as output parameters in the estimation process. Then, the estimated states are fed into the nonlinear model to iteratively calculate the RUL of the cylinder. To evaluate the effectiveness of the proposed method, scaling leakage test data, computational fluid dynamics (CFD) simulation results, and liquid rocket engine (LREs) hot test data are used. Calibration results have proved the validity and universality of the method, with the mean absolute error (MAE) for the remaining 80% useful life prediction results being less than 0.02, 0.04, and 1.10. This study can provide technical support for fault tolerance control and orbital replanning in case of control gas cylinder leaks.

1. Introduction

Liquid propellant engines are chemical propulsion systems with liquid propellant as the working medium providing most of the thrust for launch vehicles. Control gas cylinders are part of the control system. Although the pipelines between control gas cylinders and controlled valves are protected against damage, the strong shock and vibration of engines often induce leaks. Leaks can lead to pressure loss and cause control system failure [1]. Due to the fault tolerance design, the control system fails only when the cylinder pressure drops to the critical value. This way, timely and accurate estimation of the leakage area and predicting the time between the current moment to the moment of cylinder failure, i.e., RUL for fault tolerance control and orbital replanning, can significantly decrease the impact of the cylinder leakage fault on the flight missions [2].

Recently, we have carried out extensive research on the problem of leak severity estimation, and we found few studies related to cylinder leakage. However, over the years, many methods have been developed to diagnose leaks in pipelines. There are two methods for diagnosing the pipeline leakage fault, hardware based and software based. Hardware-based approaches rely on the usage of special sensors and focus on leak fault detection and location, which is difficult to achieve for a flying vehicle. Software-based methods apply computer programs to achieve leakage fault diagnosis, which can be further classified into data-driven and model-based approaches. The data-driven methods must be supported by a large amount of test data. The leakage fault of the gas cylinder is a fatigue failure caused by the shock and vibration during the engine running, and the vibration continuously acts on the cracks, maybe leading to the changing of the leakage area. Thus, the leakage areas of different tests are diverse,

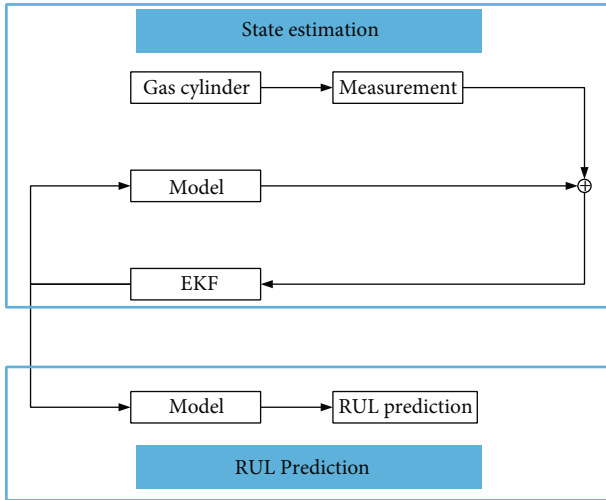


FIGURE 1: Framework of the proposed leakage estimation and RUL prediction method.

leading to different dropping rate cylinder pressure in different tests. Therefore, the data-based approach cannot accurately estimate the leakage area and RUL of the cylinder. The model-based methods can be established through the dynamic model of the system. One of the model-based methods, namely, fault model approach (FMA), enables online estimation of leakage. The main idea of this approach is based on the estimation of unmeasurable state variables associated with the leakage fault. The observer uses pressure or flow rate measurement, and no more sensors or equipment are required. In [3], the high-pressure gas pipeline was modeled as a linear parameter varying (LPV) system, and the differential Kalman filter was used as the observer to estimate the leaks. In [4], a nonlinear model derived from the water hammer equation (WHE), and the EKF observer is employed to evaluate multi leaks in pipelines. In [5], the flow rate inside the pipeline is modeled by some partial differential equations (PDEs), and the characteristic method is used to transform the PDEs into ordinary differential equations (ODEs). A robust EKF is utilized to estimate the state along with the leakage rate. In [6], the Fisher fusion method is implemented to enhance the performance of the EKF observer for leakage estimation. In [7], an EKF estimator and steady-state estimator mixed approach is proposed to improve the leakage estimation accuracy. In [8], temperature variations are considered in the WHE model, and an exact differentiation-based observer was employed to detect and isolate leaks in a plastic pipeline under temperature variations.

These studies have largely solved the problem of pipeline leakage estimation. Based on the mathematical model of pipelines and the commonly used EKF observer, unmeasurable state variables like leakage rate or leakage positions are estimated. However, the dynamic models of the pipeline are not applicable to gas cylinders. In addition, these studies are also not involved with the RUL prediction of gas cylinders. In [9], the RUL prediction methods are analyzed and defined into three main categories. The physics-based models attempt to model the evolution of the deterioration based on the mathematical models [10]. Common degrada-

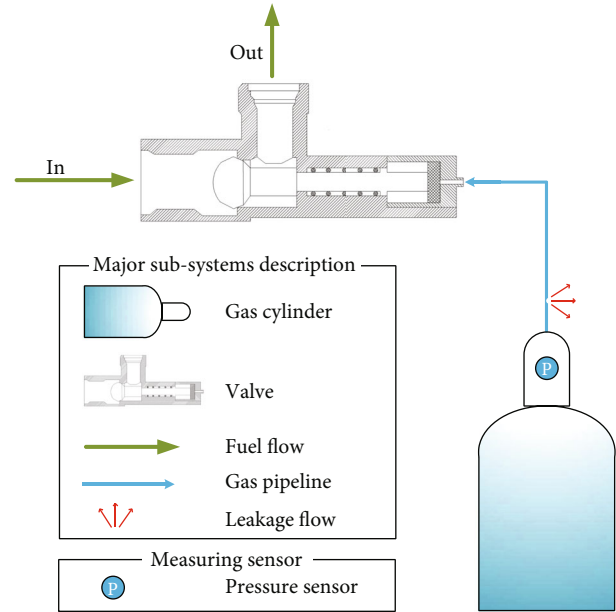


FIGURE 2: Schematic view of the gas cylinder.

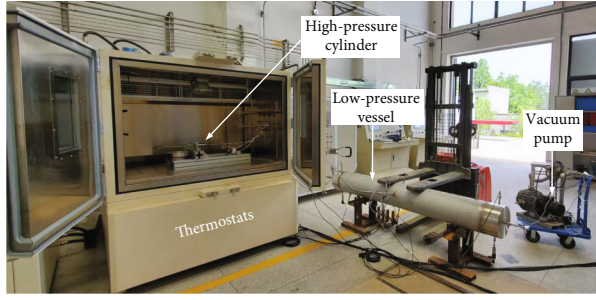
tion models include the Paris and Erdogan law [11], Forman's law [12], the Yu-Harris life equation [13], etc. The application of these models demonstrates that the degradation process of simple objects can be accurately modeled by degradation models. Therefore, a cylinder model injected with a leaky fault can be used to predict the change in cylinder pressure and thus the RUL of the cylinder. To deal with the above problems, a state representation of the gas cylinder is proposed, and the EKF is employed as a state estimator to estimate the state variables, including the leakage area. The estimated state variables of every step are used as the leakage area of the numerical model, and the four-order Runge-Kutta method is employed to estimate the RUL of the gas cylinder [14]. The main contributions of the paper are summarized below.

- (1) The mathematical model of the gas cylinder with leaks is proposed, and an EKF observer is used to estimate the leakage area
- (2) A new model-based method is proposed to predict the RUL of gas cylinders, which helps to improve the reliability of flying vehicles

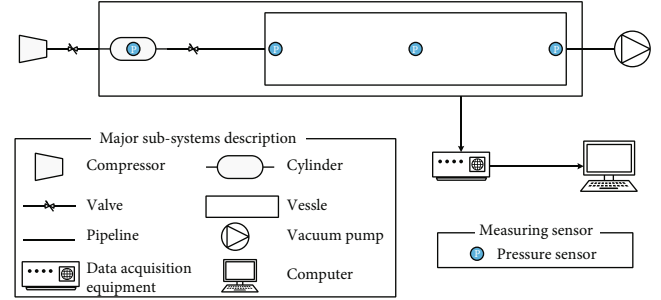
This essay's general structure is as follows: the proposed leakage estimation and RUL prediction method are introduced in Section 2, along with detailed descriptions of the experimental for method validation. The data that were used are given, and the method validation results are shown and analyzed in Section 3. Conclusions and some potential future study directions are discussed in Section 4.

2. Materials and Methods

The framework of the proposed method is shown in Figure 1, which is composed of two parts: state estimation



(a) Experimental equipment



(b) Schematic diagram of the scaling leakage test

FIGURE 3: Experimental equipment and schematic of the scaling leakage test.

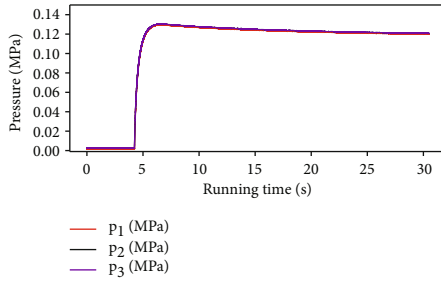


FIGURE 4: Measurement results of the pressure sensors installed in the low-pressure vessel during test 3, where p_1 and p_3 indicate the measurement results of the two pressure sensors installed on the side, and p_2 indicates the pressure sensor's measurement result in the middle.

and RUL prediction. (a) State estimation: the first step is to estimate the state based on the measurement result of the pressure sensor in the gas cylinder. By employing the EKF observer and discrete-time state-space model of the gas cylinder with leaks, the pressure and temperature of the gas cylinder and the leakage area can be estimated. If the leakage area estimation result is larger than zero, the leakage fault is detected. The estimation result of the EKF observer is further used to predict the RUL of the gas cylinder with leaks. (b) The estimation results of the pressure and temperature at every discrete-time step are used as the initial conditions, and the estimated leakage area is used as a model geometry parameter. The fourth-order Runge-Kutta method is used as the solution of the dynamic model consisting of ODEs. To get the RUL of the gas cylinder, iteratively calculate until the pressure drops to the critical pressure. The RUL equals to the number of iterative steps multiplied by the step length. At each discrete time step, this calculation is repeated to obtain the RUL at the corresponding moment.

2.1. Modeling. This section presents a model for the transient flow and leak of a gas cylinder and gives a description of the system's overall state space model.

2.1.1. Flow and Leak Modeling. The modeling process of transient pipeline flow is done and enriched in many studies [15]. However, no state space model is available for gas cylinder leakage observation. The state space model can be

derived from the dynamic model consisting of the ODEs. Therefore, this section presents a fluid dynamics-based model for a gas cylinder with leaks. Figure 2 is the schematic view of the controlling gas cylinder; the pressure of the gas cylinder can overcome the elastic force of the spring, and the friction between the spool and the valve body; then, the spool moves left, and the valve opens. Leakage in the pipeline between the gas cylinder and the valve control port can cause a continuous drop in cylinder pressure. When the cylinder pressure drops to a critical value, the spring force is greater than the sum of pressure and friction force, the valve spool moves to the right, and the valve closes.

Under the assumption of an ideal gas and adiabatic walls, the mass conservation equation, energy conservation equation, and the general gas equation are shown in Equations (1)–(3), respectively [16]:

$$\frac{dm}{dt} = -q_m, \quad (1)$$

$$\frac{d(mc_v T)}{dt} = -c_p T q_m, \quad (2)$$

$$pV = mR_g T, \quad (3)$$

where m is the mass of gas in the cylinder, q_m is the leakage rate, c_v and c_p are the specific heat capacity at constant volume and specific heat capacity at constant pressure, respectively, T is the average temperature of the gas in the cylinder, p is the average pressure of the gas in the cylinder, and R_g is the specific gas constant of the gas in the cylinder, which is given by the molar gas constant divided by the molar mass of the gas.

Based on Equations (1)–(3), the lumped-element model of the gas cylinder with leaks can be derived as follows:

$$\frac{dp}{dt} = -\frac{kR_g T}{V} q_m, \quad (4)$$

$$\frac{dT}{dt} = -\frac{(k-1)R_g T^2}{pV} q_m, \quad (5)$$

where $k = c_p/c_v$ is the capacity ratio of the gas.

TABLE 1: Detailed information of the scaling leakage test.

Parameter	Value	Units
The initial pressure of the high-pressure cylinder	>25	MPa
The initial temperature of the high-pressure cylinder	295.15	K
Volume of the high-pressure cylinder	7.5×10^{-4}	m^3
The initial pressure of the low-pressure vessel	0	MPa
Volume of the low-pressure vessel	0.15	m^3
The sampling rate of all sensors	5000	Hz
Gas type	Nitrogen	—
Leakage area	1.3×10^{-4}	m^2

For computing the leakage mass flow rate, we use the throttle element equation shown in the following:

$$q_m = A \cdot A(k) \cdot q(\lambda) \cdot \frac{p}{\sqrt{R_g T}}, \quad (6)$$

where A is the leakage area.

$$A(k) = \sqrt{k \cdot \left(\frac{2}{k+1}\right)^{(k+1)/(k-1)}}, \quad (7)$$

$$q(\lambda) = \lambda \left[\frac{k+1}{2} \cdot \left(1 - \frac{k-1}{k+1} \lambda^2\right) \right]^{1/k-1}. \quad (8)$$

λ is the velocity coefficient; when the sound speed condition shown in Equation (9) is satisfied, the flow speed at the leak hole is equal to the sound speed, and $\lambda = 1$. Due to the external pressure being low (p_b is vacuum or atmospheric pressure), Equation (9) is always satisfied.

$$\frac{p_b}{p} \leq (2/k+1)^{1/k-1}, \quad (9)$$

where p_b is the barometric pressure.

Substitute λ into Equation (8) yields the following:

$$q(\lambda) = 1. \quad (10)$$

Substitute Equations (7) and (10) into Equation (6), the leakage mass flow rate equation can be derived as shown in the following:

$$q_m = A \cdot \sqrt{k \cdot \left(\frac{2}{k+1}\right)^{(k+1)/(k-1)}} \cdot \frac{p}{\sqrt{R_g T}}. \quad (11)$$

Substitute Equation (11) into Equations (4) and (5), separately, the transient flow and leak model of the gas cylinder can be derived shown in the following:

$$\frac{dp}{dt} = -\frac{kR_g T}{V} \cdot A \cdot \sqrt{k \cdot \left(\frac{2}{k+1}\right)^{(k+1)/(k-1)}} \cdot \frac{p}{\sqrt{R_g T}}, \quad (12)$$

$$\frac{dT}{dt} = -\frac{(k-1)R_g T^2}{pV} \cdot A \cdot \sqrt{k \cdot \left(\frac{2}{k+1}\right)^{(k+1)/(k-1)}} \cdot \frac{p}{\sqrt{R_g T}}. \quad (13)$$

2.1.2. State Space Representation. Consider the discrete nonlinear system in state space with additive noise shown in the following equations:

$$\dot{\mathbf{x}}(t) = \mathbf{f}(\mathbf{x}(t)) + \mathbf{w}(t), \quad (14)$$

$$\mathbf{y}(t) = \mathbf{g}(\mathbf{x}(t)) + \mathbf{v}(t), \quad (15)$$

where \mathbf{x} is the state, \mathbf{y} is the measurement results, $\mathbf{f}(\bullet)$ and $\mathbf{g}(\bullet)$ are nonlinear mappings, \mathbf{w} and \mathbf{v} are processes and measurements of Gaussian white noise, their average values equal to zero, and covariance is denoted by \mathbf{Q} and \mathbf{R} .

Pressure and temperate of the gas cylinder and the leakage area are considered as system state variables as follows:

$$\mathbf{x} = [x_1, x_2, x_3] = [p, T, A]. \quad (16)$$

The pressure of the gas cylinder is considered as an output variable,

$$\mathbf{y} = [y_1] = [p]. \quad (17)$$

The state space representation of the gas cylinder with leaks is as follows:

$$\begin{bmatrix} \dot{x}_1(t) \\ \dot{x}_2(t) \\ \dot{x}_3(t) \end{bmatrix} = \begin{bmatrix} -\frac{kR_g x_2(t)}{V} \cdot x_3(t) \cdot \sqrt{k \cdot \left(\frac{2}{k+1}\right)^{(k+1)/(k-1)}} \cdot \frac{x_1(t)}{\sqrt{R_g x_2(t)}} \\ -\frac{(k-1)R_g x_2^2(t)}{x_1(t)V} \cdot x_3(t) \cdot \sqrt{k \cdot \left(\frac{2}{k+1}\right)^{(k+1)/(k-1)}} \cdot \frac{x_1(t)}{\sqrt{R_g x_2(t)}} \\ 0 \end{bmatrix} + \begin{bmatrix} w_1(t) \\ w_2(t) \\ w_3(t) \end{bmatrix}, \quad (18)$$

$$[y_1(t)] = [x_1(t)] + [v_1(t)]. \quad (19)$$

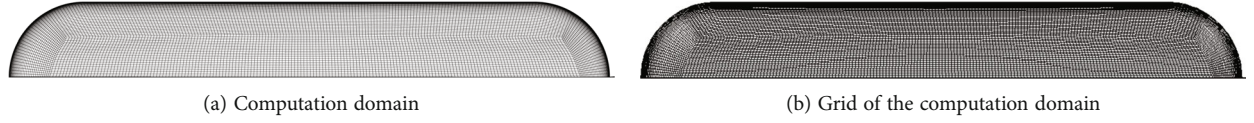


FIGURE 5: Computation domain and meshing result.

TABLE 2: Detailed information of the CFD simulation.

Parameter	Value	Units
The initial pressure of the high-pressure cylinder	20	MPa
The initial temperature of the high-pressure cylinder	273.15	K
Volume of the high-pressure cylinder	22×10^{-3}	m^3
Barometric pressure	0.101325	MPa
Time step	5×10^{-5}	s
Leakage area	1×10^{-6}	m^2
Gas type	Helium	—
Grid volume	56000	Cell
Turbulence model	RNG k- ϵ [21]	—

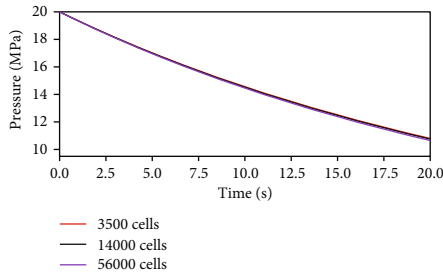


FIGURE 6: Gas cylinder leakage process simulated with different grid volumes.

2.2. Extended Kalman's Filter. The filter is the technical term for determining the system's state using the measurement results. The Kalman filter is a recursive filter that estimates the system's state [17]. Kalman's filter is based on linear systems and inappropriate in nonlinear systems. By linearizing the nonlinear system into a linear system, the use of the Kalman filter is extended to nonlinear systems, which is the extended Kalman filter (EKF) [18].

The discrete-time description derived from the continuous model shown in Equations (14) and (15) is as follows:

$$\mathbf{x}_n = \Phi(\mathbf{x}_{n-1}) + \mathbf{w}_{n-1}, \quad (20)$$

$$\mathbf{y}_n = h(\mathbf{x}_n) + \mathbf{v}_n, \quad (21)$$

where n is the discrete time and Φ and h are system and output functions.

The filtering process is given as follows:

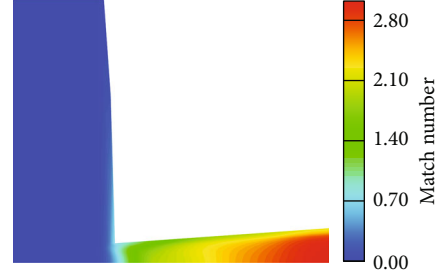


FIGURE 7: Speed distribution of leakage hole at 20 s.

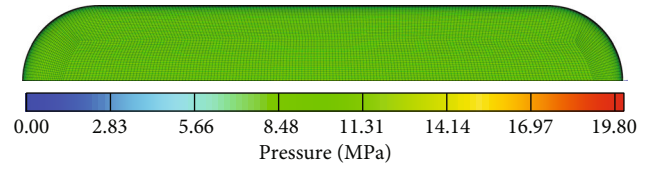


FIGURE 8: Pressure distribution of the overall computation domain at 20 s.

TABLE 3: Detailed information of the LRE hot test.

Parameter	Value	Units
The initial pressure of the gas cylinder	21	MPa
The initial temperature of the gas cylinder	293.15	K
Volume of the gas cylinder	0.022	m^3
Gas type	Helium	—
Moment of leakage failure	118.36	s
Critical pressure	11.8	MPa
The sampling rate of the pressure sensor	100	Hz
Leakage area	Unknown	m^2

Prediction equations,

$$\hat{\mathbf{x}}_n^- = \Phi(\hat{\mathbf{x}}_{n-1}^-), \quad (22)$$

$$\mathbf{P}_n^- = \mathbf{A}_{n-1} \mathbf{P}_{n-1}^- \mathbf{A}_{n-1}^T + \mathbf{Q}_{n-1}. \quad (23)$$

Update equations,

$$\hat{\mathbf{x}}_n = \hat{\mathbf{x}}_n^- + \mathbf{K}_n (\mathbf{y}_n - h(\hat{\mathbf{x}}_n^-)), \quad (24)$$

$$\mathbf{K}_n = \mathbf{P}_n^- \mathbf{C}_n^T (\mathbf{C}_n \mathbf{P}_n^- \mathbf{C}_n^T + \mathbf{R}_n)^{-1}, \quad (25)$$

$$\mathbf{P}_n = (\mathbf{I} - \mathbf{K}_n \mathbf{C}_n) \mathbf{P}_n^-. \quad (26)$$

\mathbf{P} is the estimate error covariance. \mathbf{K} is the Kalman gain. The superscript “ \wedge ” and “ $-$ ” indicate the state and the prior estimate or prediction. \mathbf{A}_{n-1} is the Jacobian matrix of the state transfer equation at step $n-1$, and \mathbf{C}_n is the Jacobian matrix

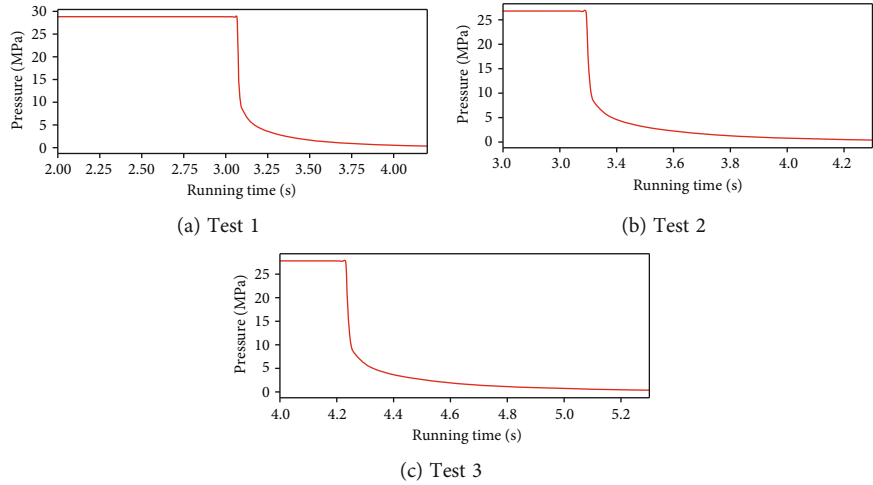


FIGURE 9: Measurement results of the pressure sensors installed in the high-pressure cylinder during three tests.

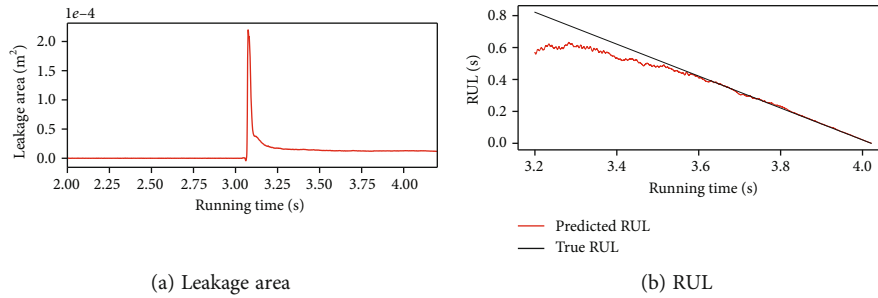


FIGURE 10: Leakage area estimation and RUL prediction results of test 1.

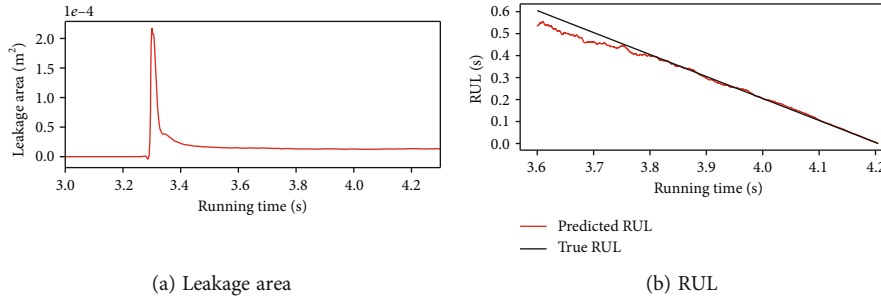


FIGURE 11: Leakage area estimation and RUL prediction results of test 2.

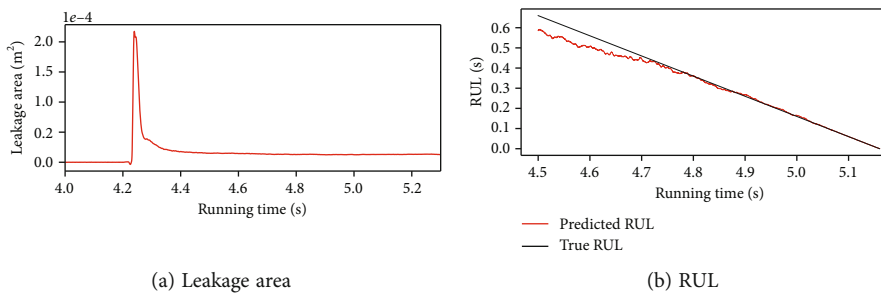


FIGURE 12: Leakage area estimation and RUL prediction results of test 3.

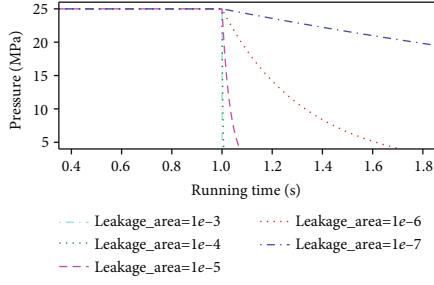


FIGURE 13: Dynamic responses of cylinder pressure under different leakage areas.

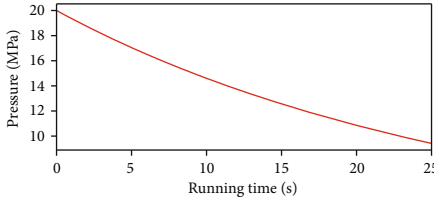


FIGURE 14: CFD simulation results of the gas cylinder under leakage fault.

of the measurement function; the definitions of A_{n-1} and C_n are as follows:

$$A_{n-1} \approx \left. \frac{\partial \Phi(\mathbf{x}_{n-1})}{\partial \mathbf{x}} \right|_{\mathbf{x}=\mathbf{x}_{n-1}}, \quad (27)$$

$$C_n \approx \left. \frac{\partial h(\mathbf{x}_n)}{\partial \mathbf{x}} \right|_{\mathbf{x}=\hat{\mathbf{x}}_n}. \quad (28)$$

2.3. Experimental Setup and Data Acquisition. To demonstrate the effectiveness of our method, the scaled leakage test is conducted, and the computational fluid dynamics (CFD) simulation is performed; in addition, the liquid rocket engine (LRE) hot-test data is also used. In this section, the experimental setup is described in detail.

2.3.1. Description of the Scaling Leakage Test. The scaling leakage test system is shown in Figure 3. The high-pressure cylinder and the low-pressure vessel are connected by piping. Before the test begins, nitrogen is charged into the high-pressure cylinder, and the low-pressure vessel is vacuumed. After the command is given, the valve in the pipeline opens, and the gas is continuously injected from the high-pressure cylinder into the low-pressure vessel. As shown in Figure 3(b), a pressure sensor is equipped in the high-pressure gas cylinder to measure the pressure change inside, and three pressure sensors are installed on both sides and in the middle of the low-pressure vessel separately to test the uniformity of pressure in the low-pressure vessel. Measurement results of the three pressure sensors installed in the low-pressure vessel during the test are shown in Figure 4, which proves that the homogeneous gas assumption is reasonable. Due to the large pressure difference between the high-pressure cylinder and the low-pressure

vessel, the sound speed flow condition shown in Equation (9) is always during the test; the pressure variation of the high-pressure cylinder of the scaling leakage test can characterize the real cylinder leakage. Detailed information of the scaling leakage test is shown in Table 1.

2.3.2. Description of the Full-Scale CFD Simulation. The computational domain of the CFD simulation is a sphere with a volume of $22 \times 10^{-3} \text{ m}^3$; the ideal gas equation and the Sutherland equation are used to describe compressibility and viscosity, respectively [19]. In addition, the adiabatic wall assumption is used. The CFD simulation of this paper is based on the Ansys fluent code, which is a widely used finite element analysis (FEA) software. The computation domain is created and discretized using ANSYS ICEM; to reduce the computation complexity, a two-dimensional axisymmetric computational domain is used, and the computation domain and meshing result are shown in Figure 5 [20]. Detailed information of the simulation is shown in Table 2. The gas cylinder leakage process simulated with different grid volumes is shown in Figure 6; as the figure shows, when the grid volume is greater than 3500 cells, the simulation results are close. The speed distribution of the leakage hole and pressure distribution of the overall computation domain are shown in Figures 7 and 8, which proves the rationality of Equation (10) and the homogeneous gas assumption.

2.3.3. Description of the LRE Hot-Test. As one of the most important subsystems of LRE, the gas generator (GG) is used to generate high-temperature and pressure gas by the combustion of fuel and oxidizer; then, the combusted gas generated by the GG is used to drive the high-pressure turbine pump (HPTP). If the combustion process is aborted, the HPTP stops turning, and the LRE shuts down. Figure 2 is the schematic view of the control gas cylinder, and the valve controlled is the fuel supply valve of GG. The control principle is detail described in Section 2.1.1. If the valve is closed to cut off the fuel supply to the GG, the combustion inside can no longer be maintained and the engine will automatically shut down. The gas cylinder leak failure occurred in over ten LRE hot tests; in one of these tests, the cylinder pressure drops to the critical value, and the LRE shuts down. Detailed information of the LRE hot test is shown in Table 3.

3. Results and Discussion

In this section, three groups of scaling leakage test data, one group of CFD simulation data, and one group of LRE hot-fire test data are used to evaluate the leakage estimation and RUL prediction capacity of the proposed method.

3.1. Calibration Results of the Scaling Leakage Test. We conducted three tests on the equipment shown in Figure 3. The change in pressure of the high-pressure cylinder during the three tests is shown in Figure 9. Figures 9(a)–9(c) correspond to the first, second, and third tests, respectively. In this paper, the first, second, and third tests are referred to as test 1, test 2, and test 3, respectively. In each subplot of Figure 9, the horizontal axis is the time axis, and the vertical axis indicates the measurement value of the pressure sensor

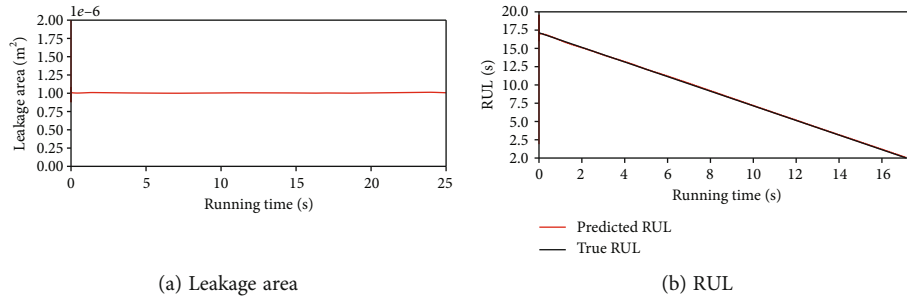


FIGURE 15: Leakage area estimation and RUL prediction results of the full-scale CFD simulation.

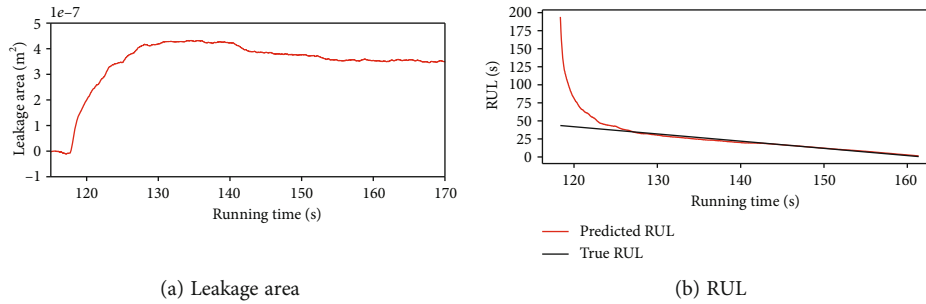


FIGURE 16: Leakage area estimation and RUL prediction results of the full-scale CFD simulation.

in the cylinder. As shown in the subplots, the three leakage tests' initial pressures and leak moments vary. However, since the test equipment is the same, the leakage area observation results should be the same.

The leakage area estimation and RUL prediction results of test 1, test 2, and test 3 are shown in Figures 10–12; the leakage area estimation results are shown in Figures 10(a), 11(a), and 12(a), and the RUL prediction results are shown in Figures 10(b), 11(b), and 12(b), for every subplot in the figures; the horizontal axis is the time axis, and the vertical axis in Figures 10(a) and (b), 11(a) and (b), and 12(a) and (b) indicate the leakage area and RUL, separately. As shown in Figure 9, the moment of leakage fault happening is different, and the initial pressure of the high-pressure cylinder before leaks is not the same. However, the leakage area estimation results shown in Figures 10(a), 11(a), and 12(a) indicate that the leakage moment is consistent with those shown in Figure 9; simultaneously, the estimated leakage areas are close to each other. The RUL prediction results are shown in Figures 10(b), 11(b), and 12(b). In the three scaling leakage tests, the critical pressure is set to 0.5 Mpa. The actual RUL of each moment is equal to the time between that moment and the critical point moment (the moment when the cylinder pressure is equal to 0.5 Mpa). The black curves represent the actual RUL, and the red curves indicate the predicted RUL. Except for the short period in the beginning, the RUL prediction results are close to the actual values. Dynamic responses of cylinder pressure under different leakage areas are shown in Figure 13, the horizontal axis is the time axis, and the vertical axis indicates the pressure; leakage faults of different leakage areas are injected to the model described in Section 2.3.1 at 1 s; it can be seen that the model can respond to the sudden leakage fault in time.

Therefore, the leakage area observation error in the beginning is due to the fluctuations of the leak area observation results after the leakage fault happened, after multiple filtering steps, the leakage area converges to a stable value. As shown in Equation (22)–(26), before the leakage fault happened, the estimate error covariance \mathbf{P} decreases with the filtering process; therefore, the Kalman gain \mathbf{K} drops to a small value resulting the filter to have minimal weight on measurement information. When a sudden leakage fault occurs, the filter tends to have a large weight on the model prediction result, which is not reasonable and causes filtering delays. In addition, the relative leakage area in the test is large, resulting in significant errors in the RUL prediction results. In [22], the strong tracking Kalman filter (STF) which combined the fading factor with EKF is proposed to track abrupt faults. However, STF may cause an overshoot for leakage area estimation [23].

3.2. Calibration Results of the Full-Scale CFD Simulation.

Simulation results of the pressure on the computing domain center are shown in Figure 14. As shown in the figure, the internal pressure of the cylinder starts to drop from 20 Mpa, and the drop rate gradually decreases.

Figure 15 shows the leakage observation results of the leakage area and prediction results of the full-scale CFD simulation. The leakage area estimation results shown in Figure 15(a) match the data in Table 2. It is demonstrated that the observer proposed in this paper can obtain accurate leakage area estimation results based on the pressure measurement result only. Figure 15(b) shows the RUL prediction result, the actual RUL of each moment is equal to the time between that moment, and the critical point moment (the moment when the cylinder pressure is equal to 11.8 Mpa);

as shown in the figure, the predicted RUL is close to the actual RUL of the cylinder.

3.3. Calibration Results of the LRE Hot-Test. Figure 16(a) shows the leakage area estimation result of the LRE hot test, as shown in the figure, the leakage area firstly increases and then decreases, while showing some fluctuation. The variation of leakage area over time in the test is due to the effect of shock and vibration on the cracked control pipeline during engine operation. The predicted RUL of the gas cylinder is shown in Figure 16(b), the actual RUL of each moment is equal to the time between that moment and the critical point moment (the moment when the cylinder pressure is equal to 11.8 Mpa), the RUL of the initial prediction is larger than the actual value, this is because of the changing of leakage area during the test, and the RUL prediction is based on the leakage area estimated. When the leakage area stopped changing drastically, the RUL prediction result turned out to be accurate.

4. Conclusions

The RUL prediction method of control gas cylinders that combines the EKF and transient flow and leak model is proposed. In this method, leakage area estimation is based on the EKF, and RUL prediction is based on the transient flow and leak model derived in this paper.

To prove the efficiency of our method, the scaled leakage test is conducted, and the computational fluid dynamics (CFD) simulation is performed; in addition, the LRE hot-test data is also used, the mean absolute error (MAE) for the remaining 80% useful life prediction results being less than 0.02, 0.04, and 1.10, separately. These works demonstrated the effectiveness of our method to predict the RUL of cylinders with different kinds of the medium under the leakage fault.

Some limitations of the current work still exist. Due to the characteristics of Kalman's filtering, there is a delay in observing the leakage area, leading to significant errors in the initial life prediction results. In addition, the variation of leakage area over time can affect the accuracy of RUL prediction results.

In our future work, we will keep researching some topics, like improving the filtering methods and modeling of the crack change process.

Nomenclature

A :	The leakage area (m^2)
A :	The Jacobian matrix of the state transfer equation
C :	The Jacobian matrix of the measurement function
c_v :	The specific heat capacity at constant volume (J/(kg.K))
c_p :	The specific heat capacity at constant pressure (J/(kg.K))
$f(\bullet)$:	Nonlinear mappings of the state transfer equation
$g(\bullet)$:	Nonlinear mappings of the measurement equation
k :	The capacity ratio of the gas
K :	The Kalman gain

m :	The mass of gas in the cylinder (kg)
p :	The average pressure of the gas in the cylinder (pa)
P :	The estimate error covariance
p_b :	Vacuum or atmospheric pressure (pa)
Q :	Covariance of the process noise matrix
q_m :	The leakage rate (kg/s)
R :	Covariance of the observation noise matrix
R_g :	The specific gas constant of the gas in the cylinder (J/(kg.K))
T :	The average temperature of the gas in the cylinder (K)
v :	Measurement Gaussian white noise
w :	Process Gaussian white noise
x :	The states
y :	The measurement results
λ :	The velocity coefficient.

Superscript

\wedge :	The state
$-$:	The prior estimate or prediction.

Acronyms

CFD:	Computational fluid dynamics
EKF:	Extended Kalman filter
FMA:	Fault model approach
FEA:	Finite element analysis
GG:	Gas generator
HPTP:	High-pressure turbine pump
LPV:	Linear parameter varying system
LRE:	Liquid rocket engine
MAE:	Mean absolute error
ODE:	Ordinary differential equations
PDE:	Partial differential equations
RUL:	Remaining useful life
STF:	Strong tracking Kalman filter
WHE:	Water hammer equation.

Data Availability

All data included in this study are available upon request by contacting the corresponding author.

Conflicts of Interest

The authors declare no conflict of interest.

References

- [1] Z. Zhang, H. Chen, Y. Gao, and H. Zhang, "Review on fault diagnosis technology of liquid rocket engine," *Journal of Propulsion Technology*, vol. 43, no. 6, article 210345, 2022.
- [2] J. Wu, "Liquid-propellant rocket engines health-monitoring-a survey," *Acta Astronautica*, vol. 56, no. 3, pp. 347–356, 2005.
- [3] J. A. Delgado-Aguíñaga, G. Besancon, O. Begovich, and J. E. Carvajal, "Multi-leak diagnosis in pipelines based on extended Kalman filter," *Control Engineering Practice*, vol. 49, pp. 139–148, 2016.
- [4] P. L. Dos Santos, T. P. Azevedo-Perdicoulis, J. A. Ramos, J. M. de Carvalho, G. Jank, and J. Milhinhos, "An LPV modeling and identification approach to leakage detection in high

- pressure natural gas transportation networks,” *IEEE Transactions on Control Systems Technology*, vol. 19, no. 1, pp. 77–92, 2011.
- [5] M. Jahanian, A. Ramezani, A. Moarefianpour, and M. Aliari Shouredeli, “Gas pipeline leakage detection in the presence of parameter uncertainty using robust extended Kalman filter,” *Transactions of the Institute of Measurement and Control*, vol. 43, no. 9, pp. 2044–2057, 2021.
- [6] R. Doshmanziari, H. Khaloozadeh, and A. Nikoofard, “Gas pipeline leakage detection based on sensor fusion under model-based fault detection framework,” *Journal of Petroleum Science and Engineering*, vol. 184, article 106581, 2020.
- [7] I. D. L. Santos-Ruiz, J. R. Bermúdez, F. R. López-Estrada, V. Puig, L. Torres, and J. A. Delgado-Aguíñaga, “Online leak diagnosis in pipelines using an EKF-based and steady-state mixed approach,” *Control Engineering Practice*, vol. 81, pp. 55–64, 2018.
- [8] O. Bektas, J. Marshall, and J. A. Jones, “Comparison of computational prognostic methods for complex systems under dynamic regimes: a review of perspectives,” *Archives of Computational Methods in Engineering*, vol. 27, no. 4, pp. 999–1011, 2020.
- [9] M. A. Bin Zaidan, *Bayesian Approaches for Complex System Prognostics*, [Ph.D. Thesis], University of Sheffield, 2014.
- [10] P. Paris and F. Erdogan, “A critical analysis of crack propagation laws,” *Journal of Basic Engineering*, vol. 85, no. 4, pp. 528–533, 1963.
- [11] C. H. Oppenheimer and K. A. Loparo, “Physically based diagnosis and prognosis of cracked rotor shafts,” in *Proceedings Volume 4733, Component and Systems Diagnostics, Prognostics, and Health Management II*, pp. 122–132, Orlando, FL, USA, 2002.
- [12] R. F. Orsagh, J. Sheldon, and C. J. Klenke, “Prognostics/diagnostics for gas turbine engine bearings,” in *Proceedings of the ASME Turbo Expo 2003, collocated with the 2003 International Joint Power Generation Conference. Volume 1: Turbo Expo 2003*, pp. 159–167, Atlanta, GA, USA, 2003.
- [13] J. A. Delgado-Aguíñaga, O. Begovich, and G. Besançon, “Exact-differentiation-based leak detection and isolation in a plastic pipeline under temperature variations,” *Journal of Process Control*, vol. 42, pp. 114–124, 2016.
- [14] J. C. Butcher, “A history of Runge-Kutta methods,” *Applied Numerical Mathematics*, vol. 20, no. 3, pp. 247–260, 1996.
- [15] R. M. Lesyshen, *Water Transmission Line Leak Detection Using Extended Kalman Filtering*, [Ph.D. Thesis], University of Saskatchewan, 2005.
- [16] P. K. Kundu, I. M. Cohen, and D. R. Dowling, *Fluid Mechanics*, Academic Press, 2015.
- [17] R. E. Kalman, “A new approach to linear filtering and prediction problems,” *Journal of Basic Engineering*, vol. 82, no. 1, pp. 35–45, 1960.
- [18] Y. Pei, S. Biswas, D. S. Fussell, and K. Pingali, “An elementary introduction to Kalman filtering,” *Communications of the ACM*, vol. 62, no. 11, pp. 122–133, 2019.
- [19] J. H. Arnold, “Vapor viscosities and the Sutherland equation,” *The Journal of Chemical Physics*, vol. 1, no. 2, pp. 170–170, 1933.
- [20] T. Stolarski, Y. Nakasone, and S. Yoshimoto, *Engineering Analysis with ANSYS Software*, Butterworth-Heinemann, 2018.
- [21] N. Koutsourakis, J. G. Bartzis, and N. C. Markatos, “Evaluation of Reynolds stress, $k-\epsilon$ and RNG $k-\epsilon$ turbulence models in street canyon flows using various experimental datasets,” *Environmental Fluid Mechanics*, vol. 12, no. 4, pp. 379–403, 2012.
- [22] X. Pu, S. Liu, H. Jiang, and D. Yu, “Adaptive gas path diagnostics using strong tracking filter,” *Proceedings of the Institution of Mechanical Engineers, Part G: Journal of Aerospace Engineering*, vol. 228, no. 4, pp. 577–585, 2014.
- [23] Z. Wei, S. Zhang, S. Jafari, and T. Nikolaidis, “Gas turbine aero-engines real time on-board modelling: a review, research challenges, and exploring the future,” *Progress in Aerospace Sciences*, vol. 121, article 100693, 2020.